



**Michigan
Technological
University**

Michigan Technological University
Digital Commons @ Michigan Tech

Michigan Tech Publications, Part 2

12-21-2023

The Influence of Boron (B), Tin (Sn), Copper (Cu), and Manganese (Mn) on the Microstructure of Spheroidal Graphite Irons

A. V. Bugten

Norges Teknisk-Naturvitenskapelige Universitet

P. Sanders

Michigan Technological University, sanders@mtu.edu

C. Hartung

Elkem Silicon Products (ESP)

R. Logan

Elkem ASA

M. Di Sabatino

Norges Teknisk-Naturvitenskapelige Universitet

See next page for additional authors

Follow this and additional works at: <https://digitalcommons.mtu.edu/michigantech-p2>



Part of the [Materials Science and Engineering Commons](#)

Recommended Citation

Bugten, A., Sanders, P., Hartung, C., Logan, R., Di Sabatino, M., & Michels, L. (2023). The Influence of Boron (B), Tin (Sn), Copper (Cu), and Manganese (Mn) on the Microstructure of Spheroidal Graphite Irons.

International Journal of Metalcasting. <http://doi.org/10.1007/s40962-023-01218-z>

Retrieved from: <https://digitalcommons.mtu.edu/michigantech-p2/327>

Follow this and additional works at: <https://digitalcommons.mtu.edu/michigantech-p2>



Part of the [Materials Science and Engineering Commons](#)

Authors

A. V. Bugten, P. Sanders, C. Hartung, R. Logan, M. Di Sabatino, and L. Michels

THE INFLUENCE OF BORON (B), TIN (Sn), COPPER (Cu), AND MANGANESE (Mn) ON THE MICROSTRUCTURE OF SPHEROIDAL GRAPHITE IRONS

A. V. Bugten and M. Di Sabatino

Department of Materials Science and Engineering, Norwegian University of Science and Technology, 7034 Trondheim, Norway

P. Sanders

Department of Materials Science and Engineering, Michigan Technological University, Houghton, MI 49931, USA

C. Hartung

Innovation Department, Elkem Silicon Products, Fiskaaveien 100, 4621 Kristiansand, Norway

R. Logan

Elkem Materials, Inc., Pittsburgh, PA, USA

L. Michels 

Innovation Department, Elkem Silicon Products, Fiskaaveien 100, 4621 Kristiansand, Norway
Department of Physics, Norwegian University of Science and Technology, 7034 Trondheim, Norway

Copyright © 2023 The Author(s)
<https://doi.org/10.1007/s40962-023-01218-z>

Abstract

Most spheroidal graphite irons (SGIs) have a matrix consisting of ferrite, pearlite, or a mix of the two. To achieve the desired matrix composition, pearlite promoters such as Mn, Cu, or Sn, are added to the molten metal. Among these elements, Sn is the most potent pearlite promoter. However, each has a different impact on the solidification, graphite precipitation, eutectoid transformation, and ultimately the final structure of the material. Research has shown that B promotes ferrite in fully pearlitic grades where Cu and Mn were used to promote pearlite. The present work investigates the effect of B in SGI with additions of Sn, Cu, and Mn, and the effects of varying amounts of the different pearlite promoters on the matrix composition. The results show that Mn alone at levels of approximately 0.9 wt% is not enough to promote a fully pearlitic matrix, while 0.5 wt% Cu combined with 0.67 wt% Mn is sufficient. Likewise, a fully pearlitic

microstructure can be obtained by alloying with 0.06 wt% Sn and 0.67 wt% Mn. B was found to promote ferrite in fully pearlitic SGI alloyed with Sn or Cu. However, in the absence of those elements, B promoted pearlite when alloyed with just Mn. Graphite protrusions were observed on the graphite nodule surface only for B-added alloys with Sn and Cu. In these cases, it is believed B promotes ferrite by changing the growth mechanism of graphite after solidification from spherical to lamellar. However, a different graphite morphology is observed when B is added with just Mn. Thermal analysis data is in agreement with the microstructural observations regarding the ferrite promoting effect of B.

Keywords: spheroidal graphite iron, SGI, ferrite, pearlite, B, Sn, Cu, Mn

This paper is an invited submission to IJMC selected from presentations at the 7th Keith Millis Symposium on Ductile Iron held October 18–20, 2023, at the Crown Plaza Atlanta Perimeter at Ravinia, Atlanta, GA. It is published in the IJMC by permission of the DIS (Ductile Iron Society).

Received: 06 November 2023 / Accepted: 09 November 2023
Published online: 21 December 2023

Introduction

Boron (B) is used to increase the hardenability of steels. Therefore, steels containing B have commonly been used for hot stamping of automobile parts since the 1980s.¹ Steel scrap is often added to the metal charge of cast iron to

reduce the carbon footprint and lower the costs of the material.²⁻⁴ However, trace levels of B are reported to have detrimental effects on the microstructure of SGI. These detrimental effects include the promotion of carbides,⁵⁻⁷ and the promotion of ferrite in pearlitic SGI.⁸⁻¹⁰ Bugten et al.⁵ investigated the possibility of B affecting the populations of nonmetallic inclusions in SGI, as the non-metallic inclusions are important for nucleation of graphite nodules,^{11,12} but no influence of B on the populations of inclusions could be found.

SGI with a fully pearlitic matrix is preferred for applications that require high strength and good wear resistance.^{7,13} The most frequently employed pearlite-promoting elements in SGI are manganese (Mn), copper (Cu), and tin (Sn). The pearlite-promoting mechanisms behind Cu and Sn have been claimed to be the formation of films covering the graphite nodules, which retards diffusion of carbon (C) from the matrix.^{6,8-10,14,15} However, multiple studies by Lacaze and Sertucha et al. have indicated that

Table 1. The Chemical Composition of the FeSi Nodularizer and Inoculant

Alloy	Type	Si [wt%]	Ca [wt%]	Al [wt%]	Mg [wt%]	Ce [wt%]
MgFeSi	Nodularizer	45.8	1.5	0.7	5.9	0.17
Ca,Al-FeSi	Inoculant	76.0	1.2	1.4	–	–

The Balance is Fe

the pearlite-promoting effects of Cu and Sn are due to other mechanisms.¹⁴⁻²³ Cu, combined with Mn, was found to decrease the growth temperature of ferrite to temperatures where the paramagnetic to ferromagnetic transformation of ferrite occurs. This significantly lowers the diffusivity of interstitial and substitutional elements in the ferrite matrix.¹⁶⁻²³ Sn is believed to substantially decrease the undercooling needed for nucleation of pearlite, which may be attributed to formation of Fe₃SnC on which cementite can nucleate.^{17,20,24,25} Using CALPHAD-based software, it has been shown that Mn significantly reduces the C-content of ferrite at the ferrite/austenite part of the Fe-Si-C-Mn phase diagram, therefore reducing the driving force for diffusion of C from austenite to graphite.^{17,18}

The ferrite promoting effect of B in pearlitic SGI has largely been investigated on the basis that diffusion barriers in the form of films exists around the graphite nodules.⁸⁻¹⁰ However, to the best of our knowledge, no consistent evidence of the existence of films of either Cu or Sn around graphite nodules are presented in literature.^{8-10,14,15} In light of the findings, presented by Lacaze et al.,¹⁴⁻²³ on the pearlite promoting mechanisms of Cu, Sn, and Mn, it is therefore believed that the studies on B in SGI alloyed with Cu (see references⁸⁻¹⁰) may be prone to misconceptions of the ferrite promoting mechanism of B.

This study investigates the influence of B, Sn, Mn, and Cu on the SGI microstructure. Various alloys with different pearlite-promoting elements are designed. For each of these alloys, an alloy with an addition of 50 ppm B is also made. Optical microscopy techniques, scanning electron

Table 2. The Bulk Chemical Composition

Sample ID	C [wt%]	Si [wt%]	Mn [wt%]	Mg [wt%]	Al [wt%]	O [wt%]	S [wt%]	N [wt%]	Sn [wt%]	Cu [wt%]	CE [wt%]	B [ppm]
Ref-0B	3.59	2.31	0.67	0.043	0.0085	0.0010	0.0075	0.0078	0.007	0.03	4.30	5
Cu-0B	3.65	2.36	0.67	0.046	0.0095	0.0010	0.0085	0.0061	0.008	0.55	4.37	6
Mn-0B	3.66	2.32	0.86	0.042	0.0086	0.0005	0.0085	0.0077	0.007	0.03	4.37	5
Sn1-0B	3.63	2.37	0.68	0.044	0.0095	0.0012	0.0079	0.0072	0.031	0.03	4.36	5
Sn2-0B	3.64	2.34	0.67	0.042	0.0092	0.0013	0.0085	0.0059	0.057	0.03	4.36	5
Sn3-0B	3.58	2.31	0.68	0.043	0.0092	0.0029	0.0084	0.0074	0.106	0.03	4.29	5
Ref-50B	3.61	2.32	0.68	0.046	0.0092	0.0036	0.0086	0.0077	0.007	0.03	4.32	44
Cu-50B	3.53	2.29	0.68	0.043	0.0089	0.0025	0.0076	0.0072	0.006	0.51	4.23	44
Mn-50B	3.58	2.33	0.91	0.045	0.0090	0.0011	0.0089	0.0071	0.006	0.03	4.29	44
Sn1-50B	3.56	2.33	0.68	0.044	0.0089	0.0011	0.0077	0.0070	0.031	0.03	4.27	43
Sn2-50B	3.61	2.35	0.68	0.044	0.0091	0.0009	0.0078	0.0076	0.060	0.03	4.33	43
Sn3-50B	3.60	2.37	0.69	0.043	0.0092	0.0009	0.0074	0.0065	0.104	0.03	4.33	43

Concentrations of other notable elements are Zr (ca. 0.0009 wt%), Ce (ca. 0.0058 wt%), La (ca. 0.0012 wt%), P (ca. 0.028 wt%), V (ca. 0.007 wt%), Nb (ca. 0.0014 wt%), Ti (ca. 0.001 wt%), Cr (ca. 0.032 wt%). Average CEs for alloys without B and with B are 4.34 and 4.30 wt%, respectively

CE is the carbon equivalent. The balance is Fe

microscopy (SEM), and thermal analysis are used to assess the influence of B and the pearlite-promoting elements on graphite nodule number density, matrix composition, and graphite surface morphology. Furthermore, microparticles high in Sn are characterized by energy-dispersive spectroscopy (EDS) in SEM.

Design of Experiment

Experimental Setup

SGI alloys in this study have been nodularized with Mg-FeSi and inoculated with a (Ca, Al)-ferrosilicon. The compositions of the alloys are shown in Table 1.

Two experimental melts were produced in a 275-kg induction furnace from 100% low alloyed cast iron returns. One of the melts was made by adding 50 ppm B. Composition adjustments were made through additions of high-purity graphite (99.9% C) and FeMn (75% Mn). For Cu and Sn additions in the crucibles, high-purity FeCu and FeSn were used. The melts were tapped at 1500 °C from the furnace into a ladle containing 1.15 wt% of a MgFeSi alloy with the composition shown in Table 1. After the Mg-FeSi treatment, the liquid was poured into six different alumina crucibles containing 0.2 wt% inoculant so that each crucible contained 32kg of iron. The liquid iron was then hold for 1 minute. After that a quenched sample (known as chill coin) was collected for chemical analysis from each crucible, and the remaining liquid was poured into tensile bars (cylinders of 30 mm diameter) and into open thermal analysis cups (36 × 36 × 40 mm). The alloy labels and compositions are shown in Table 2. The carbon equivalent is calculated as $CE = \text{wt\% C} + 0.31 \text{ wt\% Si} + 0.33 \text{ wt\% P} - 0.029 \text{ wt\% Mn} + 0.41 \text{ wt\% S}$.²⁶

The alloy labeled Ref is a reference alloy, while Cu and Mn are alloys with elevated concentrations of Cu and Mn, respectively. Alloys with three levels of Sn were made. They are Sn1, Sn2, and Sn3, adding approximately 0.03, 0.06, and 0.1 wt%, respectively. Alloys labeled with 0B and 50B are alloys without and with B-addition.

Results

The Influence of Sn, Cu, Mn, and B on the Matrix Composition

Micrographs of the reference alloys, the alloys with increased concentration of Mn, the alloys with increased concentration of Cu, and the alloys with 0.1 wt% Sn, are presented in Figure 1. The left column ((a), (c), (e) and (g)) presents alloys without addition of B, while the right column presents alloys that contain 50 ppm B ((b), (d), (f) and (h)). It can be observed that 0.9 wt% of Mn alone is not

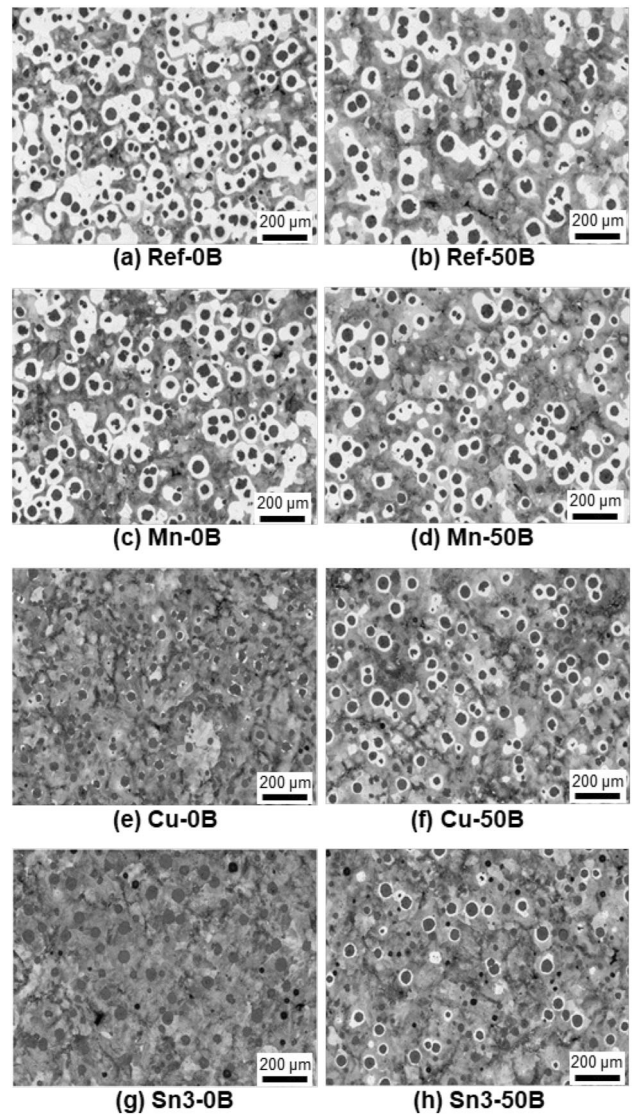


Figure 1. The influence of Mn, Cu, and Sn without B in the left column (a, c, e, and g), and alloys with 50 ppm B in the right column (b, d, f, and h).

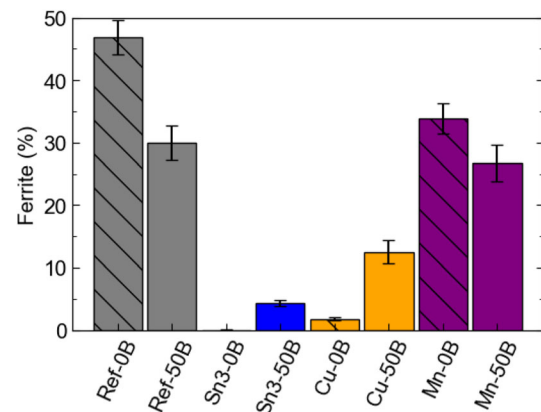


Figure 2. The effect of B, Sn, Cu and Mn on the fraction of ferrite in SGI.

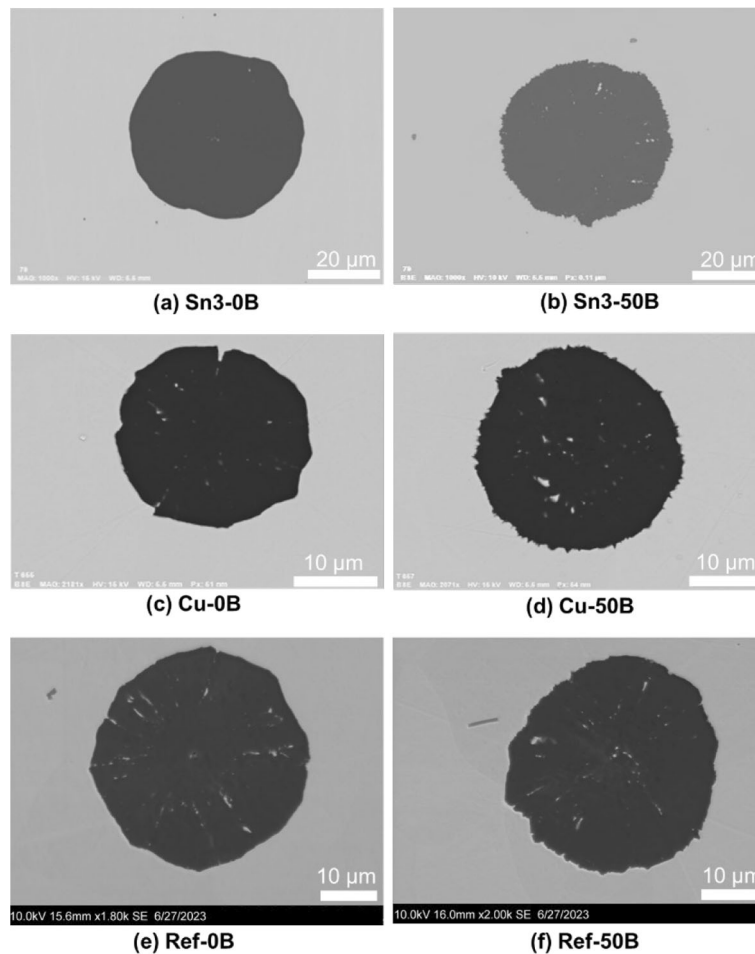


Figure 3. SEM micrographs of nodules observed in alloys with and without addition of B. (a) Sn-0B, (b) Sn-50B, (c) Cu-0B, (d) Cu-50B, (e) Mn-0B and f Mn-50B.

sufficient to obtain a fully pearlitic matrix, while a fully pearlitic matrix is obtained with a combination of 0.5 wt% Cu and 0.68 wt% Mn. A fully pearlitic matrix is also achieved with the addition of 0.1 wt% Sn and 0.68 wt% Mn. When adding 50 ppm B to the alloys, a ferrite shell appears around the nodules in the alloy with 0.5 wt% Cu and 0.67 wt% Mn. Similarly, a ferrite shell also appears for the alloy with 0.1 wt% Sn and 0.68 wt% Mn.

Figure 2 presents the measured fraction of ferrite from the alloys in Figure 1. The hatched bars represent alloys without additions of B, while the plain bars represent alloys with an addition of 50 ppm B. B promotes ferrite in the alloys which are fully pearlitic, i.e., the alloys with a combination of 0.5 wt% Cu and 0.67 wt% Mn or a combination of 0.1 wt% Sn and 0.67 wt% Mn. The fully pearlitic alloys are the alloys that contain Cu or Sn. However, B does not promote ferrite for the alloys without elevated concentrations of Cu or Sn, i.e., the reference alloy and the alloy with 0.9 wt% Mn. Instead, it seems as B promotes pearlite.

Influence of B on the Graphite Nodule Surface Morphology

Graphite nodules from the alloys Sn3, Cu and Ref are presented in Figure 3. The left column is for alloys without B, while the right column is for alloys with B. There is a significant difference in nodule surface morphology between the alloys with and without addition of B. The nodule surface morphology of all the alloys without addition of B is smooth. When B is added to the alloys protuberances appear on the nodule surface, making the surface morphology rough.

Micrographs of the protuberances observed on the graphite nodules from the alloys Sn3-50B and Ref-50B are presented in Figure 4. Figure 4(a) shows the protuberances observed in alloy Sn3-50B. The protuberances are thin and sharp. Figure 4(b) and (c) shows protuberances that appear in two different locations on the graphite nodules presented in Figure 3(f). These protuberances seem to generally be wider and not as sharp as the protuberances observed in Sn3-50B.

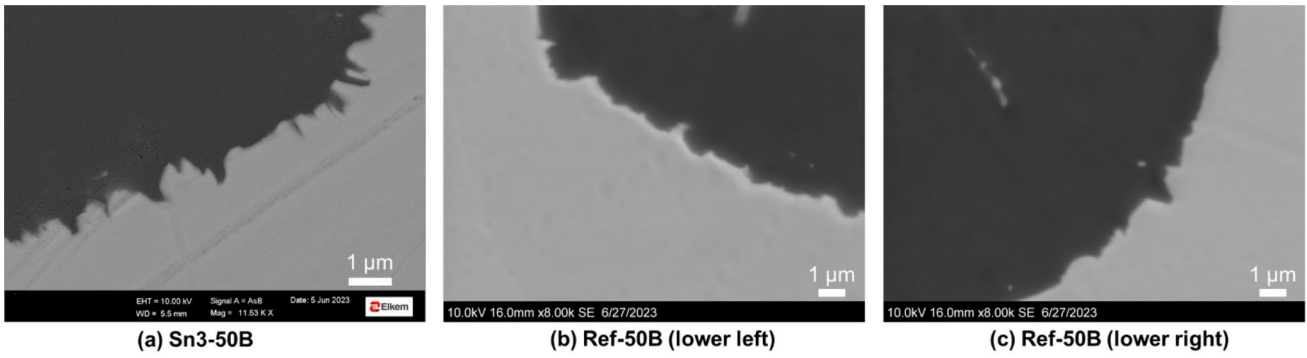


Figure 4. SEM micrographs comparing nodule surface morphologies of two of the nodules presented in Figure 3. (a) Sn3-50B, (b) Ref-50B (lower left part of nodule), and (c) Ref-50B (lower right part of nodule).

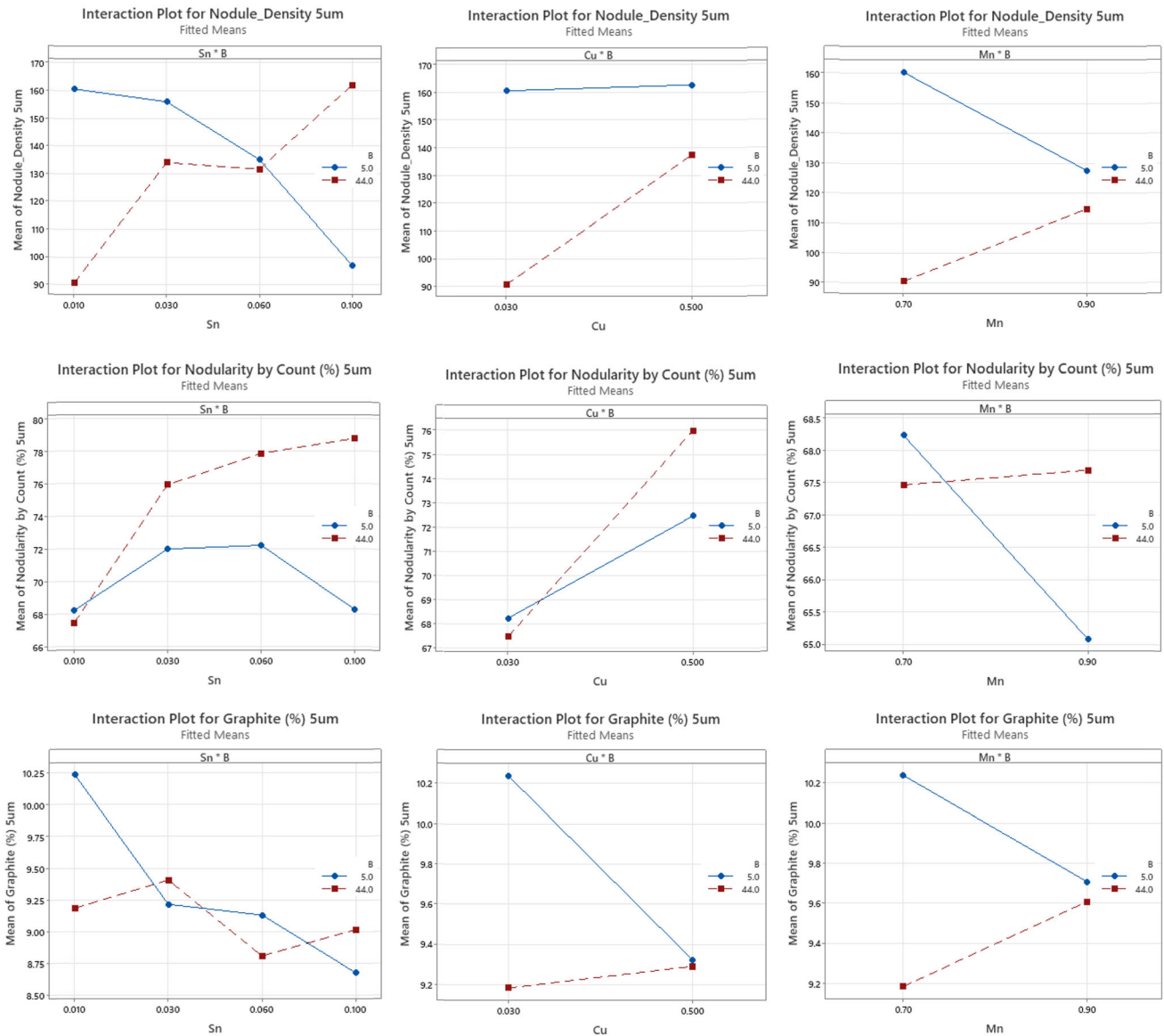


Figure 5. Two-factor interaction plots showing significant interactions at 95% confidence for nodule number density, nodularity by count, and fraction of graphite. The blue curves show alloys without addition of B, red curves are designated for alloys with B.

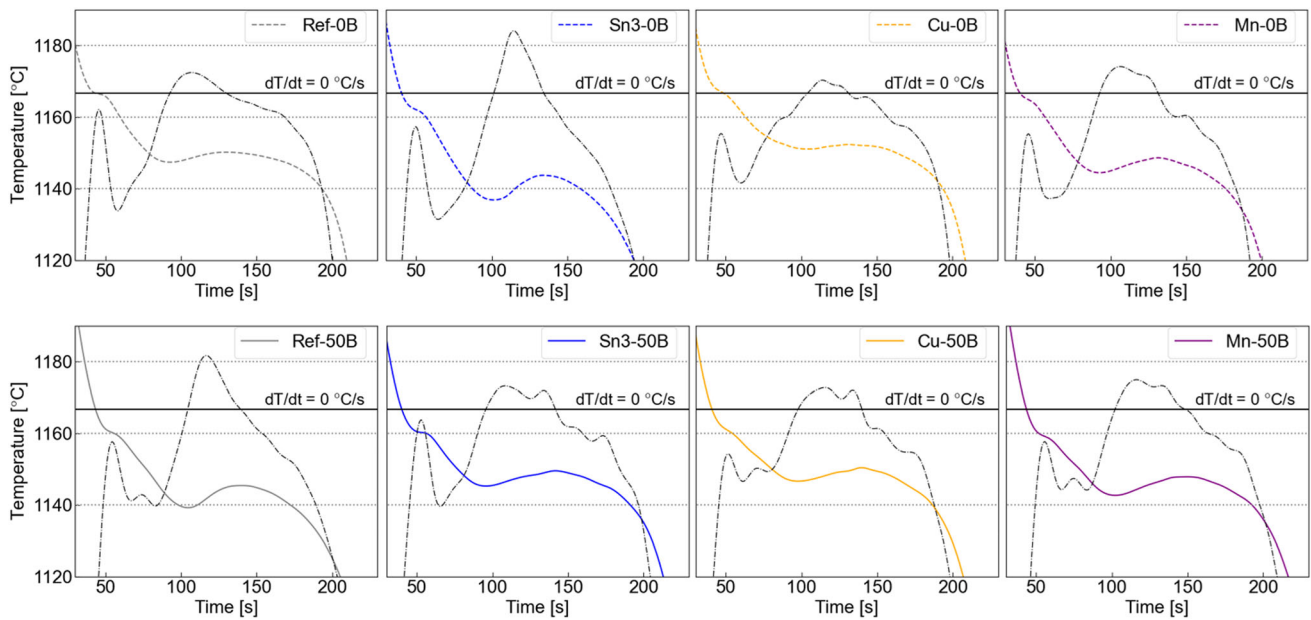


Figure 6. The influence of Sn, Cu, Mn, and B on the thermal curves up to solidification.

Influence of Sn, Cu, Mn, and B on Number Density, Nodularity, and Fraction of Graphite

The effect of Sn, Cu, Mn and B on nodule number density, nodularity, and fraction of graphite is presented in Figure 5. The measurements indicate that the nodule number density declines upon addition of Sn. Because of this, the observed influence of Sn on nodule number density is likely misleading. The nodule number density does not change significantly with increasing concentration of Cu, while for Mn, it decreases significantly. The plots indicate that B by itself reduces the nodule number density. The nodule number density increases when B is added with pearlite promoters, as evidenced by the positive slope, though the nodule number density is below the number density for the alloys without B for Cu and Mn.

The measured nodularity for the Sn-containing alloys shows little dependence on the content of Sn. Cu increases the graphite nodularity. The results for Mn are found to be statistically irrelevant when employing the two-factor approach. B by itself is found to not affect nodularity. However, when B is added together with either of the pearlite promoters Sn or Cu, the nodularity increases substantially.

The fraction of graphite is observed to decrease with increasing concentration of all pearlite formers. When B is added to the reference alloy, the fraction of graphite decreases significantly, but B is not observed to have an effect on fraction of graphite when added to either of the alloys with Sn, Cu or 0.9 wt% Mn.

Influence of Sn, Cu, Mn, and B on Thermal Curves

Figure 6 shows the influence of Sn, Cu, Mn, and B on solidification. The upper row of subfigures is for alloys without B, while the bottom row is for alloys with 50 ppm B. Each column refers to a specific pearlite element, such as 0.1 wt% Sn in column 2, or 0.5 wt% Cu in column 3. The black horizontal line shows where the first derivative is zero. The dashed black curves represent the first derivatives. One should be careful when interpreting the thermal analysis results, as they are based on open sand cups with a smaller melt volume than the cylindrical bars used for microstructure. The large difference in cooling rate makes it difficult to correlate the measured phase transformations with the microstructure of the cylindrical bars. During solid state cooling the calculated cooling rate for the quick cups was approximately 55 °C/min, while the cooling rate for the molds is usually approximately 15 °C/min.

The influence of the various elements on the thermal curves for solidification is summarized in Figure 7. The liquidus temperature (TL) decreases upon addition of Sn and Mn but is not affected significantly by addition of Cu. B is observed to reduce the liquidus in all cases.

The low eutectic temperature (TElow) decreases for Sn and Mn, while Cu increases TElow. B reduces TElow when added to the reference alloy. However, when B is added together with the pearlite promoters the TElow values of the no B and 50 ppm B alloys tends to converge.

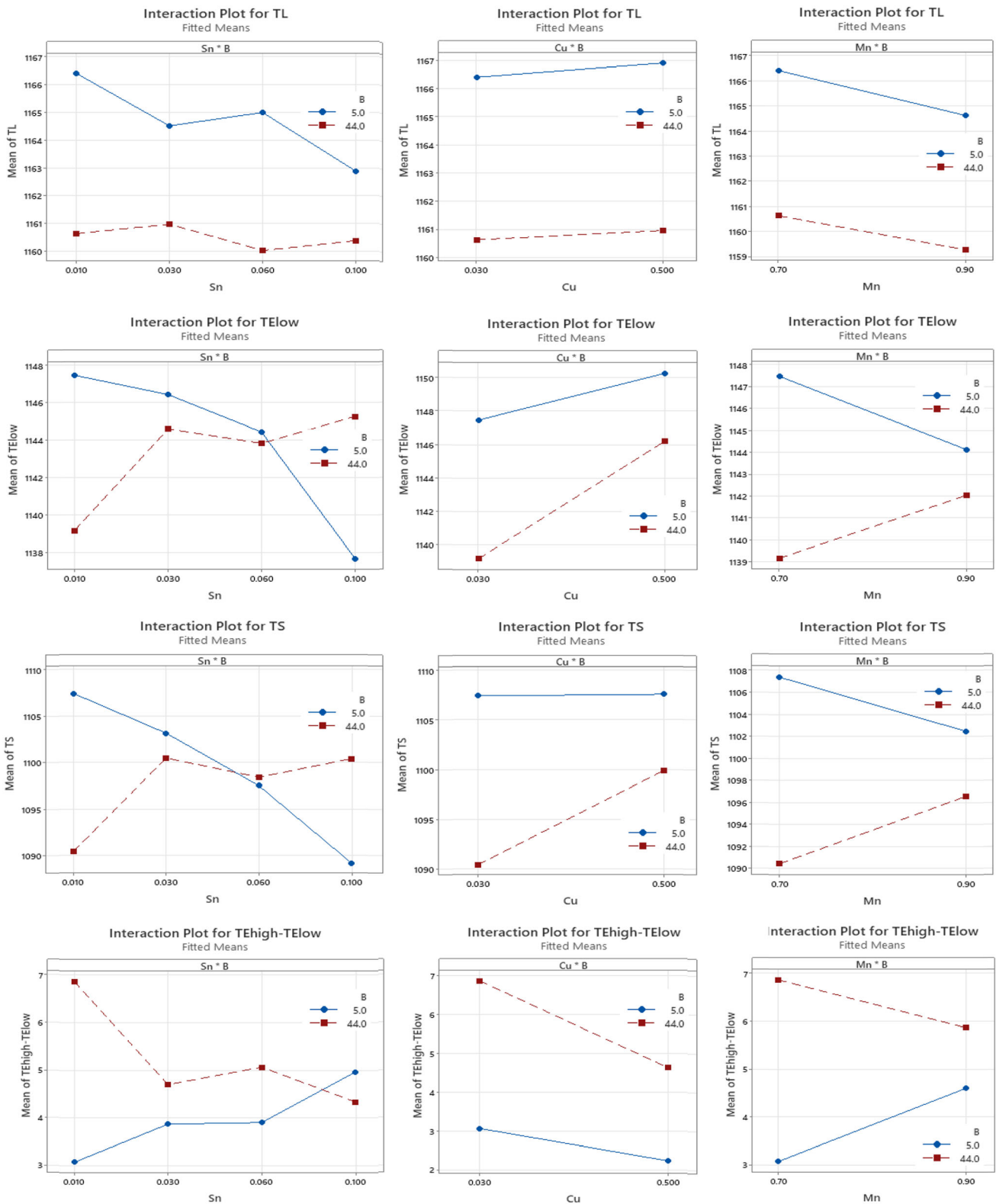


Figure 7. Two-factor interaction plots showing significant interactions at 95% confidence for influence of Sn, Cu, Mn, and B on thermal analysis variables obtained from solidification thermal curves. The blue curves show alloys without addition of B, red curves are designated for alloys with B.

The temperature at the end of solidification (TS) drops significantly when the reference alloy is alloyed with Sn or Mn, but Cu does not influence TS significantly. A

significant reduction of TS can be observed when B is added to the reference alloy. TS converges for alloys with elevated concentrations of pearlite promoters and alloys

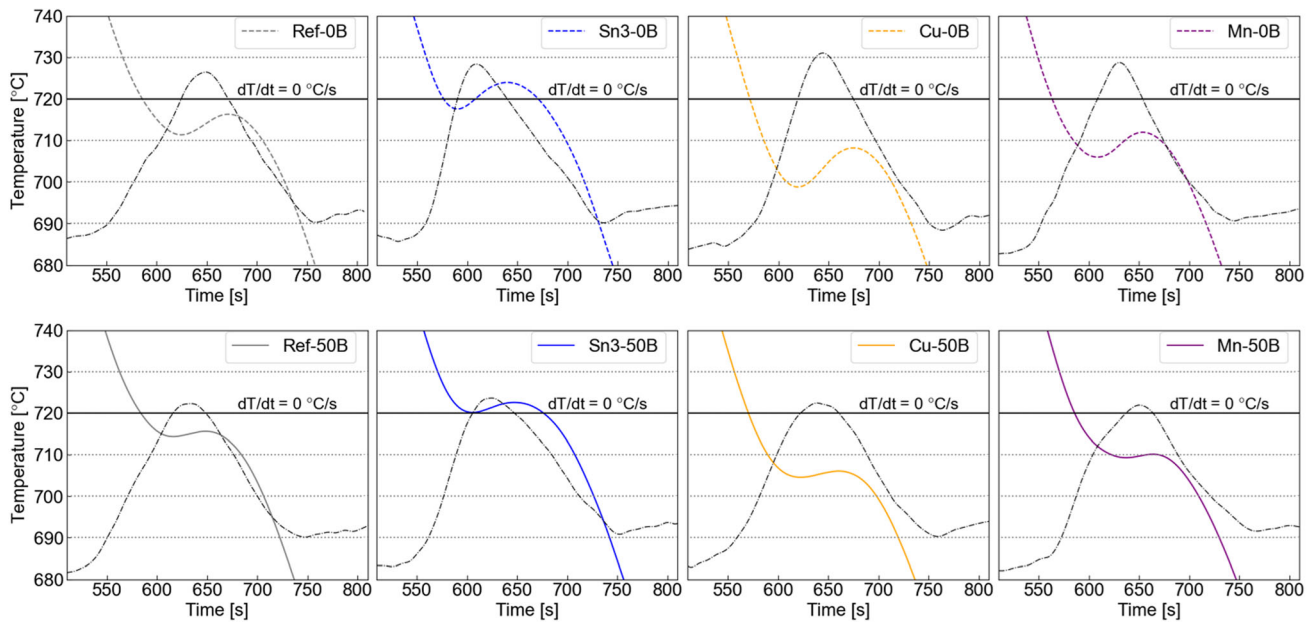


Figure 8. The influence of Sn, Cu, Mn, and B on the thermal curves of eutectoid transformation.

where B is combined with elevated concentrations of pearlite promoters.

Recalescence, $TE_{high} - TE_{low}$, increases with increasing concentration of Sn and Mn, and decreases slightly upon addition of Cu. The addition of B alone increases recalescence significantly, but when B is added together with pearlite promoters recalescence tends to converge with the values for the alloys without B.

Figure 8 shows the influence of Sn, Cu, Mn and B on the thermal curves of eutectoid transformation. The curves show that B decreases recalescence, and that B also appears to increase the low eutectoid temperature.

A two-factor analysis of the influence of B, Sn, Cu and Mn on the low eutectoid temperature, the temperature at maximum rate of temperature change (T_{trans}), and the maximum rate of temperature change during the eutectoid transformation (V_{trans}) is presented in Figure 9. The plots with white backgrounds are fitted means for data where the two-factor analysis was applied. The plots with gray background are means of the raw data, since the two-factor analysis could not be applied for these instances.

The low eutectoid temperature is observed to increase upon addition of Sn, while it decreases for addition of Cu. When the concentration of Mn is increased from approximately 0.7 wt% to 0.90 wt% the low eutectoid temperature is observed to decrease. B is observed to increase the low eutectoid temperature.

The temperature at maximum rate of temperature change (peak of dT/dt), T_{trans} , can be related to the ferrite content in SGI. Increase in ferrite content is usually associated with higher values of T_{trans} .¹⁶ Increasing the concentration of Sn increases also T_{trans} , while decreasing the concentrations of Cu and Mn both decreases T_{trans} . B is observed to increase T_{trans} .

The maximum rate of temperature change during the eutectoid transformation, V_{trans} , can also be related to the ferrite content. A decrease in V_{trans} can usually be related to a higher content of ferrite in the matrix.¹⁶ Increasing concentration of Sn lowers V_{trans} , while increasing concentrations of Cu and Mn increases V_{trans} . B is observed to decrease V_{trans} .

Particles Containing Sn

SEM investigation of alloy Sn3-0B revealed microparticles containing Sn. The microparticles are often agglomerates of various types of phases, such as the one presented in Figure 10(a). The results of the EDS point scans of the particle are shown in Table 3. It can be observed that the microparticle consists of a phase rich in Sn, Mg, and O, as shown by EDS point 1. A phase rich in Mg and O, as shown by EDS point 2. And a phase rich in Mg, O and P, as shown by EDS point 3. From the elemental mappings in Figures 10(b) through (g) it can also be observed that the phase rich in Mg, O and P, i.e., EDS point 3, also contains some Cu and S.

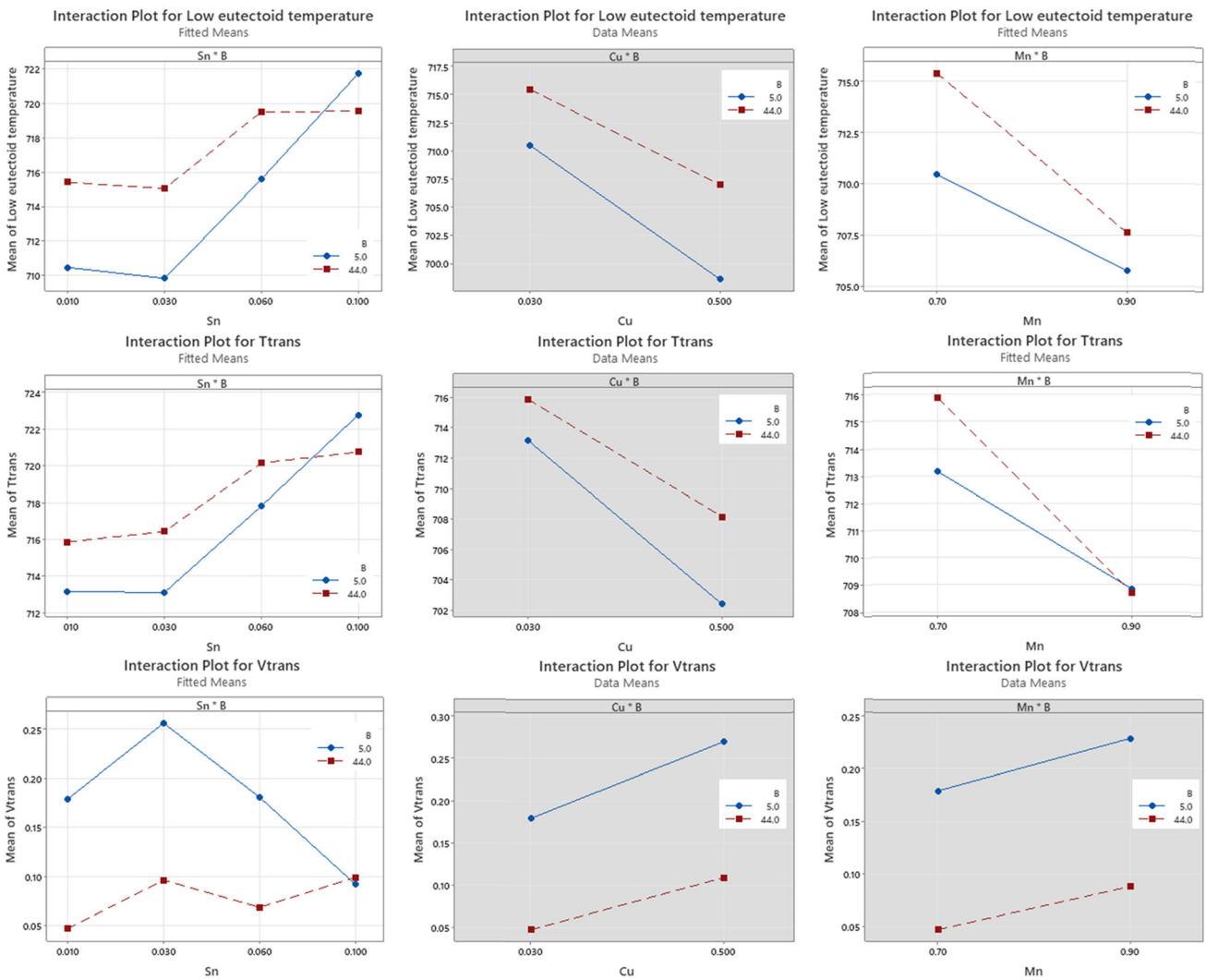


Figure 9. Various thermal analysis parameters obtained from cooling curves. The blue curves show alloys without addition of B, red curves are designated for alloys with B.

Discussion

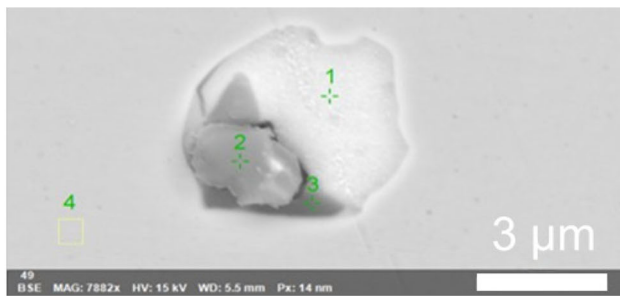
The Ferrite Promoting Mechanism of Boron

The microstructural investigation presented in Figure 3 shows that B will promote ferrite in an SGI with a fully pearlitic matrix obtained by alloying with a combination of Sn and Mn, or Cu and Mn. While in ferritic-pearlitic alloys which contain Mn, but little Cu or Sn, B is observed to promote pearlite. The observation that B promotes ferrite in alloys with Sn or Cu is in agreement with previous observations presented in studies on SGI alloyed with Sn,²⁷ and Cu.^{8–10}

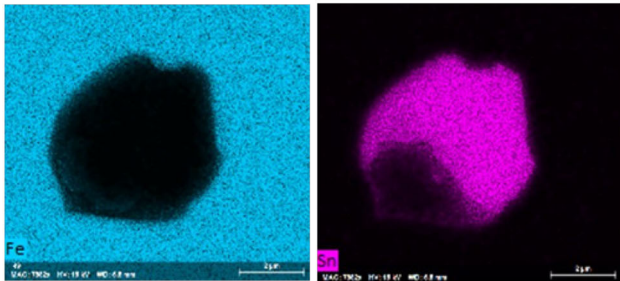
Figure 3 also shows that protuberances appear on the graphite nodule surface after addition of B. The protuberances observed on the nodules in alloys with Sn or Cu are similar to the protuberances observed in other works on

Sn²⁷ and Cu.^{8–10} These protuberances are likely flake graphite. Figure 4 presents the protuberances observed in the two alloys Sn3-50B and Ref-50B. While the protuberances in Sn3-50B are reminiscent of flake graphite, it is not clear whether the protuberances in alloy Ref-50B also are flake graphite. The protuberances in Ref-50B are wider and not as sharp as the ones observed in Sn3-50B. Further work needs to be done in order to confirm whether the protuberances observed in Ref-50B are flake graphite or a graphite morphology more akin to exploded graphite. The protuberances observed in Ref-50B are similar to the deformities observed on nodules in an alloy with 24 ppm B and 0.137 wt% Mn.⁵

The results strongly suggest that B directly affects graphite growth morphology. This could occur by B becoming absorbed by or adsorbed on the graphite crystal structure. The existence of B in graphite nodules is demonstrated by

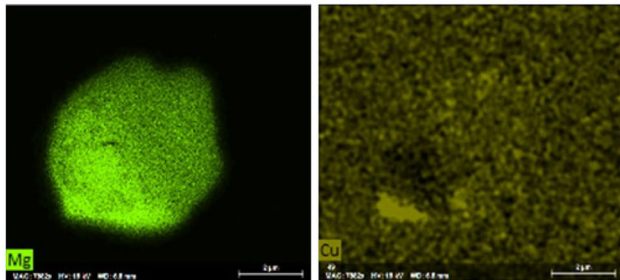


(a) BSE image



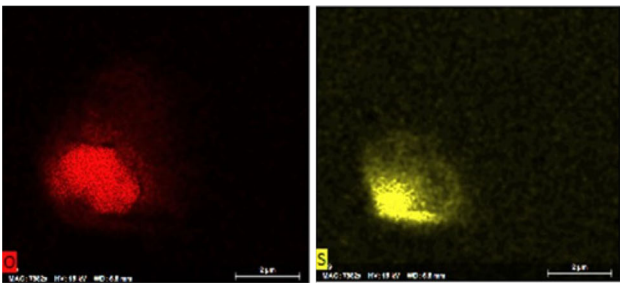
(b) Fe

(c) Sn



(d) Mg

(e) Cu



(f) O

(g) S

Figure 10. BSE micrograph and EDS elemental mappings of a Sn containing particle observed in alloy Sn3-0B.

Bugten et al., who used secondary ion mass spectrometry (SIMS) to show that B accumulates in the surface layers of the nodules.⁵ Furthermore, judging from the difference in surface morphology between the alloys with Mn and the alloys with Cu or Sn, the results suggest that also Cu and Sn may affect graphite growth morphology when B is present in the graphite. It is known that Cu segregates to the first liquid to freeze, meaning the greatest concentration of Cu in the material should be in the region around graphite nodules.²⁸ Also, Johnson and Kovacs have observed a thin layer of Sn at the graphite-iron interface using

Table 3. The EDS Point Scan Measurements from the Sn Particle Presented in Figure 5a

Position	Mg [at%]	Sn [at%]	Cu [at%]	O [at%]	P [at%]	S [at%]	Fe [at%]
1	38.9	23.3	0.0	32.0	–	–	5.8
2	26.7	1.4	0.0	65.5	–	3.0	3.5
3	65.8	4.2	1.1	16.1	1.9	1.9	9.0
4	–	–	–	–	–	–	96.0

Scanning Auger microprobe analysis.²⁹ On the other hand, Mn segregates to the last liquid to freeze, and should therefore be in relatively low concentration at the graphite-iron interface.²⁸ The observations of the segregation tendency for Cu, Sn, and Mn are in line with the observations of in which alloys with B promotes ferrite or pearlite. Lacaze et al.³⁰ have used density functional theory (DFT) calculations to investigate interaction between graphite and a set of foreign elements (C, Al, Ca, Fe, Mg, O, S, Sb, Sn, Te, and Ti). The study showed that the elements had a strong tendency to adsorb to the prismatic planes of the graphite crystal structure. The authors then propose that adsorption of foreign elements alongside Mg on the prismatic planes can interfere with the growth of graphite in the prismatic direction, meaning the newly nucleated graphite needs to protrude away from the spheroid surface. Cu has also been observed in graphite in SGI by the use of a scanning proton microprobe.³¹ It is also said that Cu-bearing irons have an increased sensitivity to influence of elements that are detrimental to graphite morphology.⁷

It is known that graphite in cast iron grows by atom attachment on the prismatic planes of the crystal structure.^{32,33} In SGI, the c-direction of the graphite normally faces the matrix during growth.³³ This means that there is limited area of prismatic planes for the C atoms to attach to for graphite growth. However, if B promotes structural changes of the nodular graphite surface and subsequent growth of flake graphite in the presence of Cu or Sn, the a-direction of the graphite crystal structure should face the matrix instead of the c-direction where the flake growth occurs on the nodule surface. The change in graphite growth from spherical to lamellar may be central to the ferrite-promoting mechanism of B because it should increase the area of prismatic planes on the nodule surface and therefore allow a higher rate of C atom attachment. This could further indicate that the rugosities observed in the alloys without Cu or Sn are not flake graphite. If the rugosities observed in alloy Mn-50B do not have the a-direction pointed toward the matrix, C atom attachment on graphite is more difficult than in the alloys with Cu or Sn, and B could then rather promote pearlite by decreasing the nodule number density. A lower number density of

nodules means longer diffusion distances, which inhibits growth of ferrite.

It is, however, important to note that alloy Sn3-0B and alloy Cu-0B are fully pearlitic, while Ref-0B and Mn-0B are ferritic-pearlitic alloys. This means that for the two alloys Ref-50B and Mn-50B (where B has been added to the material), C atoms will be able to attach to graphite regardless of the graphite morphology. This could therefore give a surface morphology that differs from nodules in a fully pearlitic alloy where Mn is used to promote pearlite without additions of Cu or Sn. Therefore, further work is necessary in order to evaluate the graphite morphology in alloys with Mn and B.

Conclusions

The influence of the steel trace element B on the microstructure of spheroidal graphite iron alloyed with the pearlite promoting elements Sn, Cu, and Mn was investigated in this study.

The main conclusion that can be drawn is that B promotes ferrite in fully pearlitic SGI alloyed with Cu or Sn. In both cases, a thicker ferrite shell was observed around the graphite nodules upon addition of 50 ppm B. The C rejected from the matrix during the ferrite-growth was deposited on the graphite nodule surface as protuberances, giving a spiky appearance of the nodule surface. It is believed that the graphite protuberances appear because B becomes incorporated in the graphite crystal structure where it interferes with graphite growth, possibly allowing Cu and Sn to also interfere. In SGI alloyed with Mn, and low concentrations of Cu and Sn, B was found to promote pearlite instead of ferrite. In the alloys without Cu or Sn, the deformities on the surface of the graphite nodules differed from the nodules in the alloys with Cu or Sn. The mechanisms behind the influence of B on graphite nodule surface morphology and SGI matrix is not understood.

The thermal analysis showed that 50 ppm of B may promote ferrite since the recalescence during the solid-state transformation decreased for all the alloys, while the temperature at the maximum rate of change of temperature during the eutectoid transformation (T_{trans}) increased, and the maximum rate of change of temperature decreased (V_{trans}).

The liquidus temperature decreased upon addition of B, suggesting B could inhibit nucleation of austenite in the melt. The recalescence during the eutectic transformation increased for the alloys without Sn, suggesting B could reduce the nucleation potential of graphite. This is in line with the measured nodule number densities, which tended to decline upon addition of B.

Sn containing microparticles were observed in the alloys with Sn. These particles have a tendency to agglomerate together with other microparticles high in Mg, Cu, and O.

Acknowledgments

This work has partly been funded by the SFI PhysMet, (Centre for Research-based Innovation, 309584). The authors gratefully acknowledge the financial support from the Research Council of Norway and the partners of the SFI PhysMet. The authors would like to thank Emmanuelle Ott, and Gro Eide from Elkem Silicon Products for their support. In addition, the authors would like to thank Eivind G. Hoel from Elkem Silicon Products for his contribution and help with the trials. This paper is an invited submission to the IJMC selected from presentations at the 7th Keith Millis Symposium on Ductile Iron held October 18–20, 2023, at the Crown Plaza Atlanta Perimeter at Ravinia, Atlanta, GA. It is published in the IJMC by permission of the DIS (Ductile Iron Society).

Funding

Open access funding provided by NTNU Norwegian University of Science and Technology (incl St. Olavs Hospital - Trondheim University Hospital).

Conflict of interest There is no conflict of interest in the manuscript.

Open Access This article is licensed under a Creative Commons Attribution 4.0 International License, which permits use, sharing, adaptation, distribution and reproduction in any medium or format, as long as you give appropriate credit to the original author(s) and the source, provide a link to the Creative Commons licence, and indicate if changes were made. The images or other third party material in this article are included in the article's Creative Commons licence, unless indicated otherwise in a credit line to the material. If material is not included in the article's Creative Commons licence and your intended use is not permitted by statutory regulation or exceeds the permitted use, you will need to obtain permission directly from the copyright holder. To view a copy of this licence, visit <http://creativecommons.org/licenses/by/4.0/>.

REFERENCES

1. E. Billur (ed.), *Hot Stamping of Ultra High-Strength Steels: From a Technological and Business Perspective* (Springer International Publishing, Cham, 2019)
2. S. Hiratsuka, H. Horie, T. Kowata, K. Koike, K. Shimizu, *Mater. Trans.* **44**, 1419–1424 (2003)
3. P. Futáš, A. Pribulová, G. Fedorko, V. Molnár, *ISIJ Int.* **57**, 374–379 (2017)
4. Z. Glavas, *Km* **50**, 75–82 (2012)
5. A.V. Bugten, L. Michels, R.B. Brurok, C. Hartung, E. Ott, L. Vines, Y. Li, L. Arnberg, M. Di Sabatino, *Metall. Mater. Trans. A* **54**, 2539–2553 (2023)

6. M. Gagné, *The sorelmetal book of ductile iron* (Rio Tinto Iron & Titanium, Montreal, Canada, 2004)
7. American foundry society: *Ductile Iron Handbook*, American foundry Society (AFS), Des Plaines, Illinois, 1992.
8. Y. Zou, M. Ogawa, H. Nakae, ISIJ Int. **52**, 505–509 (2012)
9. Y. Zou, H. Nakae, China Foundry **11**, 375–381 (2014)
10. Y. Igarashi, S. Akiyama, T. Kanno, I. Kang, H. Nakae, T. Fujikawa, J. JFS. **52**, 16–22 (2010)
11. L. Michels, A.J.F. Pires, C.A.S. Ribeiro, B. Kroka, E.G. Hoel, E. Ott, C. Hartung, Metall. Mater. Trans. B **53**, 836 (2022)
12. A. Pires, S. Simões, L. Michels, E. Ott, C. Hartung, C.S. Ribeiro, Metals. **13**(1), 5 (2022)
13. G. Cho, K. Choe, K. Lee, A. Ikenaga, J. Mater. Sci. Technol **23**, 320 (2007)
14. M. Tsujikawa, N. Matsumoto, K. Nakamoto, Y. Michiura, KEM **457**, 151–156 (2010)
15. T. Nagase, T. Maruyama, K. Asano, Y. Igarashi, Mater. Trans. **61**, 1853–1861 (2020)
16. J. Sertucha, P. Larrañaga, J. Lacaze, M. Insausti, Inter Metalcast **4**, 51–58 (2010)
17. J. Lacaze, J. Sertucha, L.M. Åberg, ISIJ Int. **56**, 1606–1615 (2016)
18. J. Lacaze, J. Sertucha, Int. J. Cast Met. Res. **29**, 74–78 (2016)
19. E. Linares, V. Gerval, J. Lacaze, Scripta Mater. **38**, 279–285 (1997)
20. J. Lacaze, J. Sertucha, M.J. Castro-Román, *From Atom Scale to Casting: A Contemporary Monograph on Cast Irons Microstructure, Open Archive Toulouse Archive Ouverte (OATAO)* (Toulouse, France, 2022)
21. R.J. Borg, J. Appl. Phys. **35**, 567–569 (1964)
22. F.S. Buffington, K. Hirano, M. Cohen, Acta Metall. **9**, 434–439 (1961)
23. J. Ågren, Scr. Metall. **20**, 1507–1510 (1986)
24. J. Lacaze, J. Sertucha, J. Phase Equilib. Diffus. **38**, 743–749 (2017)
25. J. Lacaze, J. Sertucha, P. Larrañaga, R. Suárez, Arch. Metall. Mater. **62**, 825–831 (2017)
26. D.M. Stefanescu, ASM International, and Handbook Committee: *ASM Handbook. Volume 1A, Volume 1A*, 2017
27. S.B. Pramoto, S. Hiratsuka, T. Kowata, H. Horie, T. Hareyama, J. JFS. **82**, 23–28 (2010)
28. B. Domeij and A. Diószegi: *Proceedings of the 6th Decennial International Conference on Solidification Processing*, 2017, pp. 455–58
29. W.C. Johnson, B.V. Kovacs, Met. Trans. A **9**, 219–229 (1978)
30. J. Lacaze, D. Connétable, M.J. Castro-Román, Materialia **8**, 100471 (2019)
31. F. Songlin, R. Minqin, Z. Ming, Z. Jieqing, Y. Changyi, L. Rongron, N.P.-O. Homman, K. Malmqvist, W. Yu, H. Qiyong, Nucl. Instrum. Methods Phys. Res., Sect. B **104**, 557–560 (1995)
32. D.M. Stefanescu, G. Alonso, P. Larrañaga, E. De la Fuente, R. Suarez, Acta Mater. **139**, 109–121 (2017)
33. J. Lacaze, Inter. Metalcast **11**, 44–51 (2017)

Publisher's Note Springer Nature remains neutral with regard to jurisdictional claims in published maps and institutional affiliations.